



Analysis of light scattering in the evanescent waves area by a cylindrical nanohole in a noble-metal film

Elena Eremina^{a,*}, Yuri Eremin^{b,1}, Natalia Grishina^{b,1}, Thomas Wriedt^{c,2}

^a *Universitaet Bremen, Badgasteiner Street 3, 28359 Bremen, Germany*

^b *Moscow Lomonosov State University, Lenin's Hills, 119991 Moscow, Russia*

^c *Institut für Werkstofftechnik, Badgasteiner Street 3, 28359 Bremen, Germany*

Received 11 December 2007; received in revised form 7 March 2008; accepted 11 March 2008

Abstract

The discrete sources method has been extended to analyze the scattering behavior of a cylindrical nanohole in a noble-metal film deposited on a glass prism. The dependence of the transmitted intensity on the incident angle has been investigated. Extreme transmission of the incident plane wave has been detected in the evanescent waves area.

© 2008 Elsevier B.V. All rights reserved.

Keywords: Evanescent wave; Nanohole; Extreme transmission; Discrete sources method

1. Introduction

The discovery of enhanced optical transmission through a subwavelength hole has attracted considerable interest to this optical phenomena and applications associated with nanoscale apertures in metal films [1]. The ability to localize light in spots much smaller than the volume predicted by diffraction theory offers multiple applications in biophotonics, such as probing a few molecules in a highly concentrated solution or monitoring a cell membrane with a submicrometer resolution [2,3]. Combination of a hole with other surface nanostructures or using nanohole arrays offers a wide variety of potential applications as well [4].

It is generally agreed that surface plasmon resonances play a key role in enhancing of light transmission through apertures in noble metal films [5,6]. Different groups worldwide have recently examined the transmission properties of sub-wavelength apertures. In particular, Wannemacher [1]

has studied the fundamental characteristics of a single circular nanohole in thin conducting films, as well as the role played by surface plasmon polaritons in the transmission process. Sönnichsen et al. [6] detected locally excited surface plasmons in a metal film by investigating transmission through a single nanohole using scanning near-field optical microscopy (SNOM). de Abajo [7,8] has examined light transmission through simple circular holes in perfectly conducting and real metal films, and holes containing additional structure such as a sphere or a high index dielectric filling, which seems to improve the transmission efficiency at specific wavelengths. Shuford et al. [9] have been investigating the effect of a substrate influence on the transmission properties. Degiron et al. [10] have shown that real metal plays a key role to support light transmission in a nanohole. The effect of *P*-polarized transmission efficiency has been considered by Eom et al. [11]. In the paper of Yin et al. [12] the final difference time domain (FDTD) has been used to model the problem and simulation results have been compared to experimental ones. More information regarding the transmission problem can be found in recent reviews [5,7].

In most papers mentioned above normal incidence is used as an external excitation. At the same time, there

* Corresponding author. Tel.: +49 421 218 3583; fax: +49 421 218 5378.

E-mail addresses: eremina@iwt.uni-bremen.de (E. Eremina), eremin@cs.msu.su (Y. Eremin), thw@iwt.uni-bremen.de (T. Wriedt).

¹ Tel./fax: +7 095 939 1776.

² Tel.: +49 421 218 3583; fax: +49 421 218 2507.

are multiple practical applications using an evanescent wave as external excitation [13,14]. Employing evanescent waves may allow to avoid the problem of filtering the scattered light from the refracted one. In this paper, we consider the evanescent wave scattering properties of a single sub-wavelength hole in a noble-metal film filled by a dielectric medium. The discrete sources method (DSM) [15] has already been applied to model light scattering by different nanoobjects on a plane surface [14,16]. In this paper, the DSM is adjusted to model evanescent light scattering of a fixed wavelength by a nanohole. The influence of the incident angle on the scattering properties of the hole is investigated. The effects of the size and filling of the hole, as well as the material and thickness of the metal film are considered.

In the next chapter, we present the theoretical outlines of the DSM. In the third chapter the numerical algorithm is presented and computer simulation results are discussed in the last chapter of the paper.

2. Mathematical model

Let an axially symmetric hole occupying a certain domain D_i with a smooth boundary ∂D be situated inside a film of thickness d , which is bounded by the planes Σ_1 and Σ_f . The plane Σ_1 separates the film and the substrate (glass prism). We denote the prism domain by D_1 and ambient space exterior to the film and the hole by D_0 . The upper half-space D_0 and the interior of the hole D_i are filled with water. Let us introduce a Cartesian coordinate system $Oxyz$ by choosing its origin O at the prism-surface Σ_1 in the center of the hole and O_z axis is directed into domain D_0 . The plane $z = 0$ corresponds to the Σ_1 plane (Fig. 1). We assume that the exciting field $\{\mathbf{E}^0, \mathbf{H}^0\}$ is a plane wave propagating from D_1 at the angle θ_1 with respect to the z -axis.

Then the mathematical statement of the scattering problem can be formulated as follows:

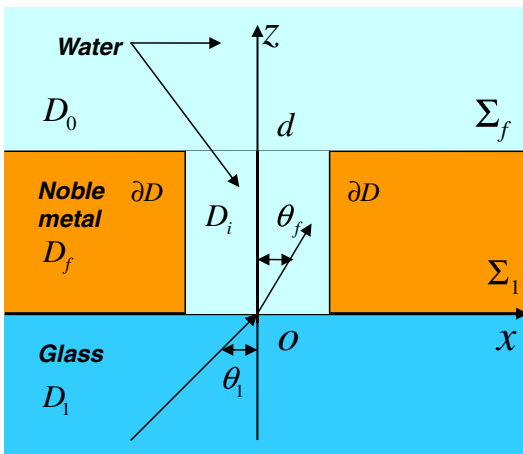


Fig. 1. Model geometry.

$$\nabla \times \mathbf{H}_\zeta = jk\varepsilon_\zeta \mathbf{E}_\zeta; \quad \nabla \times \mathbf{E}_\zeta = -jk\mu_\zeta \mathbf{H}_\zeta \text{ in } D_\zeta,$$

$$\zeta = 0, 1, f, i,$$

$$\begin{aligned} \mathbf{n}_p \times (\mathbf{E}_i(p) - \mathbf{E}_f(p)) &= 0, \\ \mathbf{n}_p \times (\mathbf{H}_i(p) - \mathbf{H}_f(p)) &= 0, & p \in \partial D; \\ \mathbf{e}_z \times (\mathbf{E}_f(p) - \mathbf{E}_1(p)) &= 0, \\ \mathbf{e}_z \times (\mathbf{H}_f(p) - \mathbf{H}_1(p)) &= 0, & p \in \sum_1; \\ \mathbf{e}_z \times (\mathbf{E}_0(p) - \mathbf{E}_f(p)) &= 0, \\ \mathbf{e}_z \times (\mathbf{H}_0(p) - \mathbf{H}_f(p)) &= 0, & p \in \sum_f \end{aligned} \quad (1)$$

and radiation/attenuation conditions at infinity for the scattered field at $z \neq 0, d$.

Here, \mathbf{e}_z is the unit normal vector to the surfaces $\Sigma_{1,f}$, \mathbf{n}_p is the outward unit normal vector to ∂D , $k = \omega/c$ and $\{\mathbf{E}_\zeta, \mathbf{H}_\zeta\}$ stands for the total field in the corresponding domain D_ζ , $\zeta = 0, 1, f, i$. While in $D_{1,f}$ the total field consists of incident and reflected waves, in D_0 the total field includes the transmitted wave which transforms to the evanescent one under certain conditions. If $\text{Im} \varepsilon_\zeta, \mu_\zeta \leq 0$ (the time dependence for the fields is chosen as $\exp\{j\omega t\}$) and the particle surface is smooth enough: $\partial D \subset C^{(2,\alpha)}$, then the above boundary-value scattering problem is uniquely solvable [17].

We construct an approximate solution to the scattering problem (1) based on the DSM [14]. First, the plane wave $\{\mathbf{E}^0, \mathbf{H}^0\}$ scattering problem on the interface is solved. The result yields external excitation fields $\{\mathbf{E}_\zeta^0, \mathbf{H}_\zeta^0\}$, $\zeta = 0, 1$ in domains $D_{0,1}$, which satisfy the transmission conditions at the plane interface. Let us construct the approximate solution of the boundary value problem (1) for the scattered field $\{\mathbf{E}_\zeta^s, \mathbf{H}_\zeta^s\}$ in D_ζ , $\zeta = 0, f, 1$ and the total field in D_i .

In the frame of DSM [15] the approximate solution is constructed by representing the electromagnetic fields as a finite linear combination of the electric and magnetic fields of multipoles distributed over an axis of symmetry inside the scatterer. Besides, the fields analytically satisfy the transmission conditions enforced at the plane interfaces $\Sigma_{1,f}$, which provides an opportunity to account for whole interactions between scatterer and interface. Then the approximate solution satisfies Maxwell equations in the domains D_ζ , $\zeta = 0, 1, f, i$, the infinity conditions and the transmission conditions at plane interfaces $\Sigma_{1,f}$. Thus, the scattering problem is reduced to the problem of approximation of the exciting field on the hole surface ∂D . Only the amplitudes of the discrete sources (DS) are to be determined from the boundary conditions at ∂D . Which can be rewritten in the following form

$$\mathbf{n}_p \times (\mathbf{E}_i - \mathbf{E}_f^s) = \mathbf{n}_p \times \mathbf{E}_f^0 \quad \mathbf{n}_p \times (\mathbf{H}_i - \mathbf{H}_f^s) = \mathbf{n}_p \times \mathbf{H}_f^0. \quad (2)$$

Prior to the construction of an approximate solution for the scattered field, the plane wave diffraction problem on the layered structure must be solved. The field representation can be written as

$$\mathbf{E}_f^{P,S} = W_i^{P,S} \mathbf{E}_f^+ + W_r^{P,S} \mathbf{E}_f^-, \quad \mathbf{H}_f^{P,S} = W_i^{P,S} \mathbf{H}_f^+ + W_r^{P,S} \mathbf{H}_f^-. \quad (3)$$

Where

$$W_i^{P,S} = \frac{T_{1f}^{P,S}}{1 - R_{f1}^{P,S} R_{f0}^{P,S} e^2}, \quad W_i^{P,S} = -\frac{T_{1f}^{P,S} R_{f0}^{P,S} e^2}{1 - R_{f1}^{P,S} R_{f0}^{P,S} e^2},$$

$$e = \exp\{-ik_f d \cos \theta_f\}.$$

Here $R_{\tau l}^{P,S}, T_{\tau l}^{P,S}$ are corresponding Fresnel reflecting and transmission coefficients from D_τ to D_l for P/S -polarized plane wave [18].

To construct the fields of dipoles and multipoles that analytically satisfy the transmission conditions at the plane interfaces $\Sigma_{1,f}$ we incorporate the Green's tensor for a stratified interface [19].

An approximate solution of the scattering problem is constructed taking into account not only the rotational symmetry of the scattering problem geometry (hole together with layered interface) but the polarization of the exciting field [15] as well. For a P -polarized excitation the field's components in (3) accept the following form:

$$\mathbf{E}_f^\pm = (\pm \cos \theta_f \mathbf{e}_x + \sin \theta_f \mathbf{e}_z) \chi^\pm \quad \mathbf{H}_f^\pm = -n_f \mathbf{e}_y \chi^\pm$$

$$\chi^\pm = \exp\{-ik_f(x \sin \theta_f \pm z \cos \theta_f)\}$$

In accordance with [14] for P -polarized excitation the following electric and magnetic vector potentials corresponding to the multipoles are used:

$$\begin{aligned} \mathbf{A}_{mn}^{e,f} &= \{g_m^e(q, w_n) \cos(m+1)\varphi; \\ &\quad -g_m^e(q, w_n) \sin(m+1)\varphi; \\ &\quad -f_{m+1}(q, w_n) \cos(m+1)\varphi\}, \end{aligned}$$

$$\begin{aligned} \mathbf{A}_{mn}^{h,f} &= \{g_m^h(q, w_n) \sin(m+1)\varphi; \\ &\quad g_m^h(q, w_n) \cos(m+1)\varphi; \\ &\quad -f_{m+1}(q, w_n) \sin(m+1)\varphi\}, \end{aligned}$$

$$\mathbf{A}_n^{e,f} = \{0; 0; g_0^h(q, w_n)\}.$$

Here, the Fourier harmonics of the Green tensor $g_m^{e,h}, f_m$ in contrast to [14] accept the form of Weyl–Sommerfeld integrals:

$$\begin{aligned} g_m^{e,h}(q, w_n) &= \int_0^\infty J_m(\lambda \rho) v_{11}^{e,h}(z, w_n, \lambda) \lambda^{1+m} d\lambda, \\ f_m(q, w_n) &= \int_0^\infty J_m(\lambda \rho) v_{31}(z, w_n, \lambda) \lambda^{1+m} d\lambda. \end{aligned} \quad (4)$$

Here, J_m is the cylindrical Bessel function, the point $q = (\rho, z)$ belongs to the half-plane $\varphi = \text{const}$, and the multipoles are distributed along the axis of symmetry $w_n \in O_z$ inside D_i . In this case, the spectral functions $v_{11}^{e,h}, v_{31}^{e,h}$ are given by

$$v_{11}^{e,h}(z, w_n, \lambda) = \begin{cases} A_{11}^{e,h}(\lambda, w_n, d) \exp\{-\eta_0|z-d|\}, & z > d \\ \frac{\exp\{-\eta_0|z-d|\} + B_{11}^{e,h} \exp\{-\eta_f|z-d|\}}{\eta_f} \\ \quad + C_{11}^{e,h} \exp\{-\eta_f z\}, & d > z > 0 \\ D_{11}^{e,h}(\lambda, w_n, d) \exp\{-\eta_f z\}, & z < 0; \end{cases}$$

$$v_{31}^{e,h}(z, w_n, \lambda) = \begin{cases} A_{31}^{e,h}(\lambda, w_n, d) \exp\{-\eta_0|z-d|\}, & z > d \\ B_{31}^{e,h} \exp\{-\eta_f|z-d|\} \\ \quad + C_{31}^{e,h} \exp\{-\eta_f z\}, & d > z > 0 \\ D_{31}^{e,h}(\lambda, w_n, d) \exp\{\eta_f z\}, & z < 0. \end{cases}$$

Here, $\eta_\zeta^2 = \lambda^2 - k_\zeta^2$, $k_\zeta^2 = k^2 \varepsilon_\zeta \mu_\zeta$, $\zeta = 0, f$.

The spectral coefficients A, B, C, D are determined from the following one-dimensional transmission conditions at $\Sigma_{1,f}(z=0, d)$ [14]:

$$\begin{aligned} [v_{11}^e] &= \left[\frac{1}{\mu} \frac{\partial v_{11}^e}{\partial z} \right] = 0, \quad [v_{11}^h] = \left[\frac{1}{\varepsilon} \frac{\partial v_{11}^h}{\partial z} \right] = 0, \\ \left[\frac{1}{\mu} v_{31}^e \right] &= 0, \quad \left[\frac{\partial v_{31}^e}{\partial z} \right] = - \left[\frac{1}{\varepsilon \mu} \right] v_{11}^e, \quad \left[\frac{1}{\varepsilon} v_{31}^h \right] = 0, \\ \left[\frac{\partial v_{31}^h}{\partial z} \right] &= - \left[\frac{1}{\varepsilon \mu} \right] v_{11}^h. \end{aligned}$$

Here, square brackets $[\]$ stay for the jump of values across the interface. In particular, the equality $v_{31}^e = v_{31}^h$ holds at $d > z > 0$.

For the total fields inside the hole the same representation as in [14] is used.

Then for the scattered fields in $D_{0,f,1}$ which satisfy the transmission conditions at Σ , the following representation is valid

$$\begin{aligned} \mathbf{E}_{\zeta,N}^s &= \sum_{m=0}^M \sum_{n=1}^{N_m} \left\{ p_{mn} \frac{j}{k \varepsilon_\zeta \mu_\zeta} \nabla \times \nabla \times \mathbf{A}_{mn}^{e,\zeta} + q_{mn}^{\frac{1}{\varepsilon_\zeta}} \nabla \times \mathbf{A}_{mn}^{h,\zeta} \right\} \\ &\quad + \sum_{n=1}^{N_0} r_n^{\frac{j}{k \varepsilon_\zeta \mu_\zeta}} \nabla \times \nabla \times \mathbf{A}_n^{e,\zeta}; \\ \mathbf{H}_{\zeta,N}^s &= \frac{j}{k \mu_\zeta} \nabla \times \mathbf{E}_{\zeta,N}^s(M), \zeta = 0, f, 1. \end{aligned} \quad (5)$$

The approximated solution for the S -polarized excitation can be constructed in a similar way. The field's components from (3) accept the form

$$\mathbf{E}_f^\pm = \mathbf{e}_y \chi^\pm, \quad \mathbf{H}_f^\pm = n_f (\pm \cos \theta_f \mathbf{e}_x + \sin \theta_f \mathbf{e}_z) \chi^\pm.$$

The following electric and magnetic vector potentials corresponding to the multipoles are employed:

$$\begin{aligned} \mathbf{A}_{mn}^{e,f} &= \{g_m^e(q, w_n) \sin(m+1)\varphi; \\ &\quad g_m^e(q, w_n) \cos(m+1)\varphi; \\ &\quad -f_{m+1}(q, w_n) \sin(m+1)\varphi\}, \\ \mathbf{A}_{mn}^{h,f} &= \{g_m^h(q, w_n) \cos(m+1)\varphi; \\ &\quad -g_m^h(q, w_n) \sin(m+1)\varphi; \\ &\quad -f_{m+1}(q, w_n) \cos(m+1)\varphi\}, \\ \mathbf{A}_n^{e,f} &= \{0; 0; g_0^e(q, w_n)\}. \end{aligned}$$

Then for the scattered fields in $D_{0,1}$, which satisfy the transmission conditions at Σ , the following representation is valid:

$$\begin{aligned} \mathbf{E}_{\zeta,N}^s &= \sum_{m=0}^M \sum_{n=1}^{N_m} \left\{ p_{mn} \frac{j}{k \varepsilon_\zeta \mu_\zeta} \nabla \times \nabla \times \mathbf{A}_{mn}^{e,\zeta} + q_{mn} \frac{1}{\varepsilon_\zeta} \nabla \times \mathbf{A}_{mn}^{h,\zeta} \right\} \\ &\quad + \sum_{n=1}^{N_0} r_n \frac{j}{k \varepsilon_\zeta \mu_\zeta} \nabla \times \nabla \times \mathbf{A}_n^{e,\zeta}; \\ \mathbf{H}_{\zeta,N}^s &= \frac{j}{k \mu_\zeta} \nabla \times \mathbf{E}_{\zeta,N}^s(M), \zeta = 0, f, 1. \end{aligned} \quad (6)$$

The completeness of the system of dipoles and multipoles guarantees the convergence of the approximate solutions (5) and (6) to the exact one [20].

3. Numerical scheme of the DSM

In this section, a short description of the numerical realization of the computational algorithm is given. As mentioned above, representations (5) and (6) satisfy all the conditions of the scattering problem (1) except the transmission conditions at the hole's surface (2). These conditions are used to determine the unknown amplitudes of discrete sources $\{p_{nm}, q_{nm}, r_n\}$. Since the scattering problem geometry is axially symmetric with respect to the Z-axis and the DS are distributed over the axis of symmetry, fulfilling the transmission conditions (2) at the surface ∂D can be reduced to a sequential set of 1D transmission problems for the Fourier harmonics of the fields. Thus, instead of matching the fields on the scattering surface (see Eq. (2)), we match their Fourier harmonics separately by reducing the approximation problem on the surface ∂D to a set of 1D problems enforced at the particle surface generatrices \mathfrak{Z} . By solving these problems one can determine the DS amplitudes.

Various numerical schemes for the amplitudes evaluation have been suggested. It has been found that more stable results can be obtained by using the generalized point-matching technique and a pseudo-solution of corresponding over-determined system of linear equations [21]. DSM is a direct method and therefore it allows solving the scattering problem for the entire set of incident angles θ_1 and for both polarizations (P and S) at once. This is an advantage compared to methods similar to discrete dipole approximation (DDA) or finite difference time domain (FDTD) which require application of an iterative scheme. Besides, the DSM numerical scheme provides an opportunity to control the actual convergence of the approximate solution to the exact one by posterior error estimation [15].

After the amplitudes of the DS have been determined, one can calculate the far field pattern $\mathbf{E}_\infty(\theta, \varphi)$ of the scattered field, which is determined at the upper semi-sphere $\Omega = \{0^\circ \leq \theta \leq 90^\circ, 0^\circ \leq \varphi \leq 360^\circ\}$ and is given by

$$\mathbf{E}_0^s(M)/|\mathbf{E}^0(z=0)| = \frac{\exp\{-jk_0 r\}}{r} \mathbf{E}_\infty(\theta, \varphi) + o(r^{-1}),$$

$$z > d, \quad r = |M| \rightarrow \infty.$$

We asymptotically estimate the Weyl–Sommerfeld integrals involved in (4) [21], which yields the following representation for the θ, φ -components of the far field pattern corresponding to representation (5)

$$E_{\infty, \theta}^P(\theta, \varphi) = \frac{jk_0}{\varepsilon_0} \sum_{m=0}^M (jk_0 \sin \theta)^m \cos(m+1)\varphi$$

$$\times \sum_{n=1}^{N_m} \{p_{nm} [\bar{g}_{nm}^e \cos \theta + jk_0 \sin^2 \theta \bar{f}_{nm}] + q_{nm} \bar{g}_{nm}^h\}$$

$$- \frac{jk_0}{\varepsilon_0} \sin \theta \sum_{n=1}^{N_0} r_n \bar{g}_{n0}^h,$$

$$E_{\infty, \varphi}^P(\theta, \varphi) = -\frac{jk_0}{\varepsilon_0} \sum_{m=0}^M (jk_0 \sin \theta)^m \sin(m+1)\varphi$$

$$\times \sum_{n=1}^{N_m} \{p_{nm} \bar{g}_{nm}^e + q_{nm} [\bar{g}_{nm}^h \cos \theta + jk_0 \sin^2 \theta \bar{f}_{nm}]\}.$$
(7)

For S -polarized excitation following to representation (6) one gets

$$E_{\infty, \theta}^S(\theta, \varphi) = \frac{jk_0}{\varepsilon_0} \sum_{m=0}^M (jk_0 \cos \theta)^m \cos(m+1)\varphi$$

$$\sum_{n=1}^{N_m} \{p_{nm} [\bar{g}_{nm}^e \cos \theta + jk_0 \sin^2 \theta \bar{f}_{nm}] - q_{nm} \bar{g}_{nm}^h\},$$

$$E_{\infty, \varphi}^S(\theta, \varphi) = \frac{jk_0}{\varepsilon_0} \sum_{m=0}^M (jk_0 \cos \theta)^m \sin(m+1)\varphi$$

$$\sum_{n=1}^{N_m} \{p_{nm} \bar{g}_{nm}^e - q_{nm} [\bar{g}_{nm}^h \cos \theta + jk_0 \sin^2 \theta \bar{f}_{nm}]\}$$

$$+ \frac{jk_0}{\varepsilon_0} \sin \theta \sum_{n=1}^{N_0} r_n \bar{g}_{n0}^h.$$
(8)

Where the corresponding spectral functions $\bar{g}_{nm}^{e,h}, \bar{f}_{nm}$, in contrast to [14], accept the form

$$\bar{g}_{nm}^{e,h}(\theta) = jk_0 \cos \theta \exp\{jk_0 d \cos \theta\} A_{11}^{e,h}(k_0 \sin \theta, z_n, d),$$

$$\bar{f}_{nm}(\theta) = jk_0 \cos \theta \exp\{jk_0 d \cos \theta\} A_{31}^e(k_0 \sin \theta, z_n, d).$$

Hence, after the unknown amplitudes of DS are determined, the far field patterns for P/S polarization (7) and (8) are represented as finite linear combinations of elementary functions. This circumstance ensures a low costs computer analysis of the scattering characteristics in the far zone.

4. Numerical results and discussion

The differential scattering cross-section (DSC) is calculated as:

$$I^{P,S}(\theta_1, \theta, \varphi) = |E_{\infty, \theta}^{P,S}(\theta_1, \theta, \varphi)|^2 + |E_{\infty, \varphi}^{P,S}(\theta_1, \theta, \varphi)|^2, \quad (9)$$

where $E_{\infty, \theta, \varphi}^{P,S}(\theta_1, \theta, \varphi)$ are the components of the far field pattern for a P (7) and S (7) polarized incident wave, in a spherical coordinate system θ, φ .

We will mostly consider the transmission cross-section (TCS), which represents the integrated intensity transmitted into the upper semi-sphere $\Omega = \{0^\circ \leq \theta \leq 90^\circ, 0^\circ \leq \varphi \leq 360^\circ\}$:

$$\sigma^{P,S}(\theta_1) = \int_{\Omega} I^{P,S}(\theta_1, \theta, \varphi) d\omega. \quad (10)$$

Next, we will present some numerical results obtained using the DSM model and discuss them shortly. As it has already been pointed out before, we used P/S -polarized plane wave excitation (6). We consider the scattering properties of the hole excited by a light source with a wavelength of $\lambda = 532$ nm. The refractive indices are: $n_1 = 1.52$

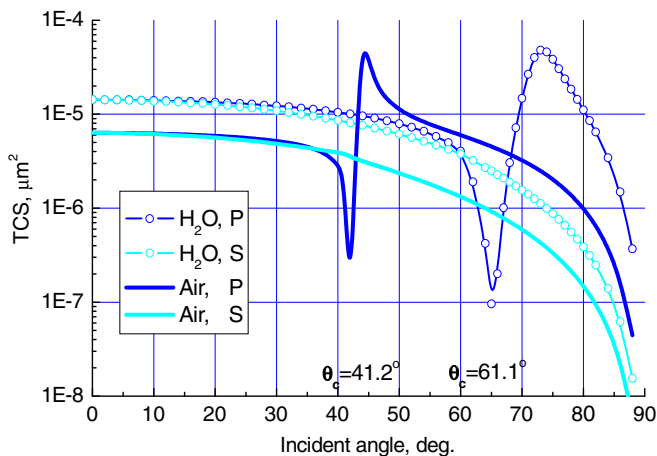


Fig. 2. Transmission cross-section (TCS) for the hole of diameter $D = 30$ nm in silver (Ag) film of thickness $d = 40$ nm in cases of air and water inside the hole.

for glass in D_1 and $n_0 = n_i = 1.33$ for water in $D_{0,i}$. As film materials silver (Ag) with refractive index $n_{Ag} = 0.15 - 3.19j$ and gold (Au) with $n_{Au} = 0.45 - 2.41j$ [22] have been chosen.

In Fig. 2 the TCS (10) versus incident angle is presented for a hole of diameter $D = 30$ nm in an Ag film of thickness $d = 40$ nm for two different cases: when both the upper half-space and the hole are filled with water or air. From the figure one can see, that the S-polarized curve monotonically decreases but the curve for P-polarization drops down beyond the critical angle (see water $\theta_c = 61.1^\circ$) and then rapidly jumps up two orders in value. A similar behaviour can be observed in the case of air near the critical angle of $\theta_c = 41.2^\circ$. Besides, the maximum value of $\sigma^P(\theta_1)$ achieved in the region of evanescent waves excitation exceeds the TCS under normal incidence $\sigma^P(0^\circ)$ almost by an order.

To analyse the scattering behaviour of the scattered intensity in the incident plane under different incident angles, the DSC was calculated for the same hole in case

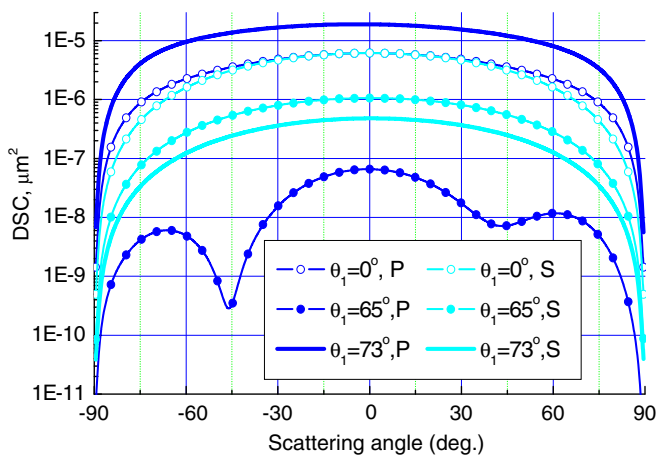


Fig. 3. Differential scattering cross-section (DSC) for the hole, $D = 30$ nm in Ag film, $d = 40$ nm versus incident angles θ_1 .

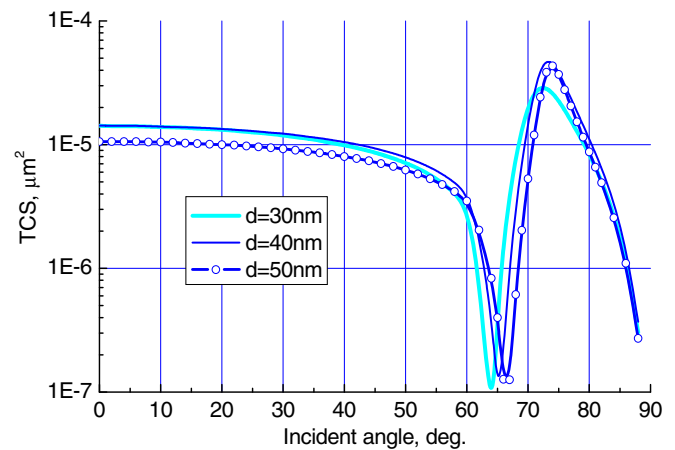


Fig. 4. TCS for P-polarized light for the hole $D = 30$ nm in Ag films of different thicknesses.

of a water filling. The results are presented in Fig. 3. For this analysis three different incident angles have been chosen: $\theta_1 = 0^\circ, 65^\circ, 73^\circ$. One can see, that the DSC for P-polarization at $\theta_1 = 73^\circ$ corresponding to the TCS maximum considerably exceeds the DSC at $\theta_1 = 65^\circ$, where the TCS achieves its minimum value (see Fig. 2).

Let us now have a closer look at the influence of the film parameters on the scattering behaviour of the TCS. In Fig. 4 the results of calculation of the TCS for P-polarized excitation for the same hole in Ag films of different thicknesses are presented. The curves demonstrate similar behaviour as in Fig. 2.

In Fig. 5 similar results but for different film materials (Au and Ag) are presented for both polarizations. From the analysis one can see, that the Ag film provides a much higher intensity peak than the Au one. We will now restrict our consideration just to an Ag film of $d = 40$ nm and investigate the influence of the hole's diameter.

In Fig. 6 the results for holes of different diameters are presented. From the results it is clear, that the larger the hole, the higher the transmitted intensity peak is, but the

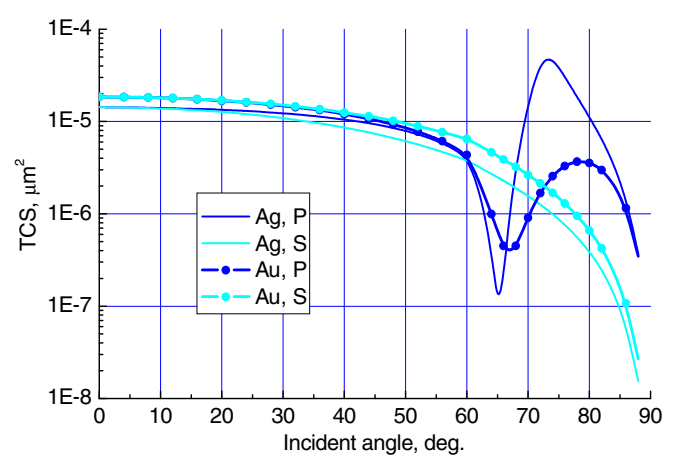


Fig. 5. TCS for P- and S-polarized lights for the hole $D = 30$ nm in Ag films of $d = 40$ nm.

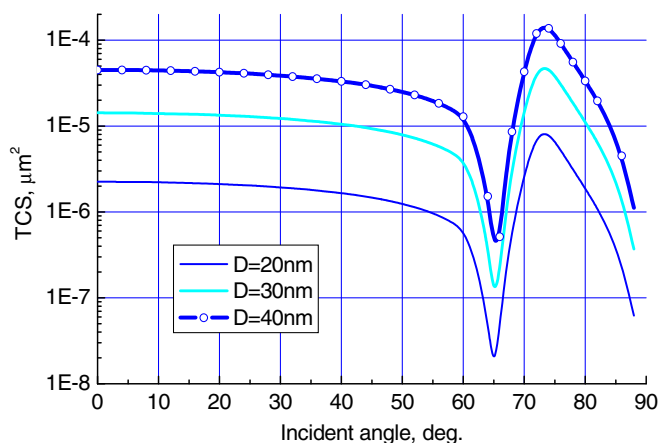


Fig. 6. TCS for P -polarized light for the holes of different diameters in Ag film, $d = 40$ nm.

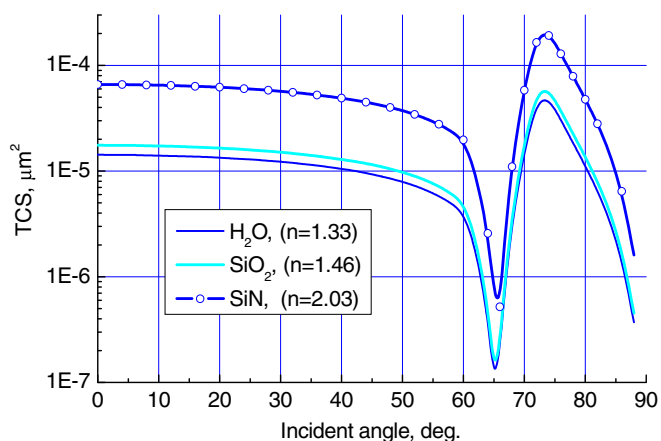


Fig. 7. TCS for P -polarized light for the hole of $D = 30$ nm in Ag film of $d = 40$ nm with different hole fillings.

curves shapes stay almost the same. We now consider how the filling of the hole affects the TCS. We take now silicon dioxide SiO_2 with a refractive index of $n_i = 1.46$, and SiN with $n_i = 2.03$. In Fig. 7 the TCS for P -polarization for the same hole is presented for the three different filling materials. From the diagrams one can see that in general the transmitted intensity peak increases together with increase of the refractive index value of the filling.

To conclude our discussion, we should emphasize, that the light scattering properties of a hole in a noble-metal film in the evanescent waves area extremely dependent on the incident angle. When the incident angle exceeds the critical one the intensity of transmitted light drops down by several orders and then sharply jumps up by several orders (Figs. 4 and 6). The position of the TCS maximum and minimum values can be slightly manipulated by varying the film parameters, material and thickness (Figs. 4 and 5), but does not depend on the hole's diameter and filling (Figs. 6 and 7). Their positions are determined by the value of the critical angle only.

5. Conclusion

In this paper, the DSM has been adjusted to scattering analysis of a single subwavelength nanohole in a noble-metal film deposited on a glass prism. The main result of this research consists of the following: extreme transmission of P -polarized scattered intensity in the evanescent waves area has been detected. The influence of the film thickness, material and the diameter and filling of the hole on this effect was investigated and discussed. The effect of extreme transmission seems to be interesting for different applications in nanooptics and biophotonics, including optical antennas and biosensors.

Acknowledgements

We gratefully acknowledge funding of this research by Deutsche Forschungsgemeinschaft (DFG) and the Russian Foundation for Basic Research (RFBR).

References

- [1] R. Wannemacher, *Opt. Comm.* 195 (2001) 107.
- [2] H. Rigneault, J. Capoulade, J. Dintinger, et al., *Phys. Rev. Lett.* 95 (2005) 117401.
- [3] T.A. Laurence, S. Weiss, *Science* 299 (2003) 667.
- [4] C. Genet, T.W. Ebbesen, *Nature* 225 (2007) 39.
- [5] W.L. Barnes, A. Dereux, T.W. Ebbesen, *Nature* 424 (2003) 824.
- [6] C. Sönnichsen, A.C. Duch, G. Steininger, M. Koch, G. von Plessen, J. Feldmann, *Appl. Phys. Lett.* 76 (2) (2000) 140.
- [7] F.J.G. de Abajo, *Rev. Modern Phys.* 79 (2007) 1267.
- [8] F.J.G. de Abajo, *Opt. Express* 10 (25) (2002) 1475.
- [9] K.L. Shuford, S.K. Gray, M.A. Ratner, G.C. Schatz, *Chem. Phys. Lett.* 435 (2007) 123.
- [10] A. Degiron, H.J. Lezec, N. Yamamoto, T.W. Ebbesen, *Opt. Comm.* 239 (2004) 61.
- [11] G.S. Eom, D. Yang, S. Lee, S. Park, Y. Lee, J.W. Hahn, *J. Appl. Phys.* 101 (2007) 103101.
- [12] L. Yin, V.K. Vasko-Vlasov, A. Rydh, et al., *Appl. Phys. Lett.* 85 (3) (2004) 467.
- [13] E. Eremina, N. Grishina, Y. Eremin, L. Helden, T. Wriedt, *J. Opt. A: Pure Appl. Opt.* 8 (2006) 999.
- [14] E. Eremina, Y. Eremin, T. Wriedt, *Opt. Comm.* 267 (2) (2006) 524.
- [15] Yu.A. Eremin, *J. Comm. Technol. Electronics* 45 (2) (2000) 269.
- [16] E. Eremina, Y. Eremin, T. Wriedt, *Opt. Comm.* 273 (1) (2007) 278.
- [17] D. Colton, R. Kress, *Inverse Acoustic and Electromagnetic Scattering Theory*, Springer, Berlin, 1992.
- [18] W.C. Chew, *Waves and Fields in Inhomogeneous Media*, IEEE Press, NY, 1995.
- [19] J.A. Kong, *Electromagnetic Wave Theory*, EMW Publishing, Cambridge, MA, 2000.
- [20] A. Doicu, Yu. Eremin, T. Wriedt, *Acoustic and Electromagnetic Scattering Analysis using Discrete Sources*, Academic Press, London, 2000.
- [21] Y. Eremin, N. Orlov, A. Sveshnikov, in: T. Wriedt (Ed.), *Generalized Multipole Techniques for Electromagnetic and Light Scattering*, Elsevier Science, Amsterdam, 1999, p. 39.
- [22] D.W. Lynch, W.R. Hunter, Comments on the optical constants of metal and an introduction to the data for several metals, in: E.D. Palik (Ed.), *Handbook of Optical Constants of Solids*, vol. 1, Academic Press, San Diego, 1985.